

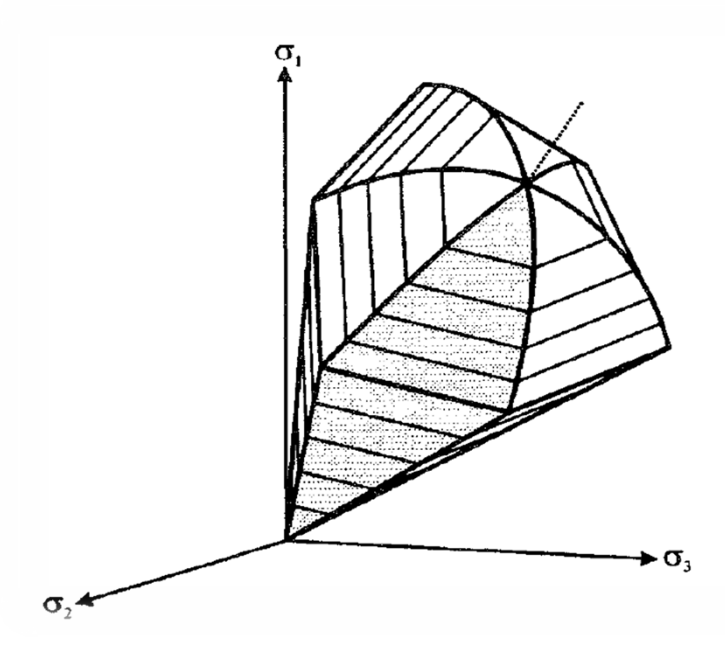
To see the latest GeoStudio learning content, visit <u>Seequent Learning Centre</u> and search the catalogue for "GeoStudio".

## Introduction

This example demonstrates how to parameterize the Hardening Soil constitutive model from laboratory data. The parameters are then used in numerical simulations of the laboratory tests and the simulated results are compared with the measured data and analytical solutions.

#### **Formulation**

A brief overview of the Hardening Soil formulation is provided as a prerequisite to the parameterizing procedure. Details of the formulation are presented in the reference book (Seequent ULC, 2024). The Hardening Soil model comprises two yield surfaces: one that resembles a hexagonal cone and a second that resembles the tip of an ellipsoid (Figure 1). The shear surface predominately governs the response to changes in deviatoric stress while the cap predominately governs the response to increments in mean effective stress. The model implemented in SIGMA/W comprises a smoother cap then what is depicted in Figure 1 (Seequent ULC, 2024).



Hardening soil yield surfaces in principal stress space Reference: Schanz et al. (1999)

Figure 1. Shear and cap yield surfaces of the Hardening Soil model (Schanz et al. (1999).

Note the following in reference to Figure 2:

- 1. The mode's formulation inherently comprises a Mohr-Coulomb failure criteria. The q:p' stress path therefore reaches the Mohr-Coulomb failure surface.
- 2. The  $^{q:\epsilon_1}$  stress-strain path is approximated by a hyperbolic curve. The characteristics of this curve are determined by some stress-dependent stiffness parameters including the initial tangent stiffness  $^{E_i}$ , which is related to the half-failure secant stiffness  $^{E_{50}}$ , and unloading-reloading stiffness  $^{E_{ur}}$ .



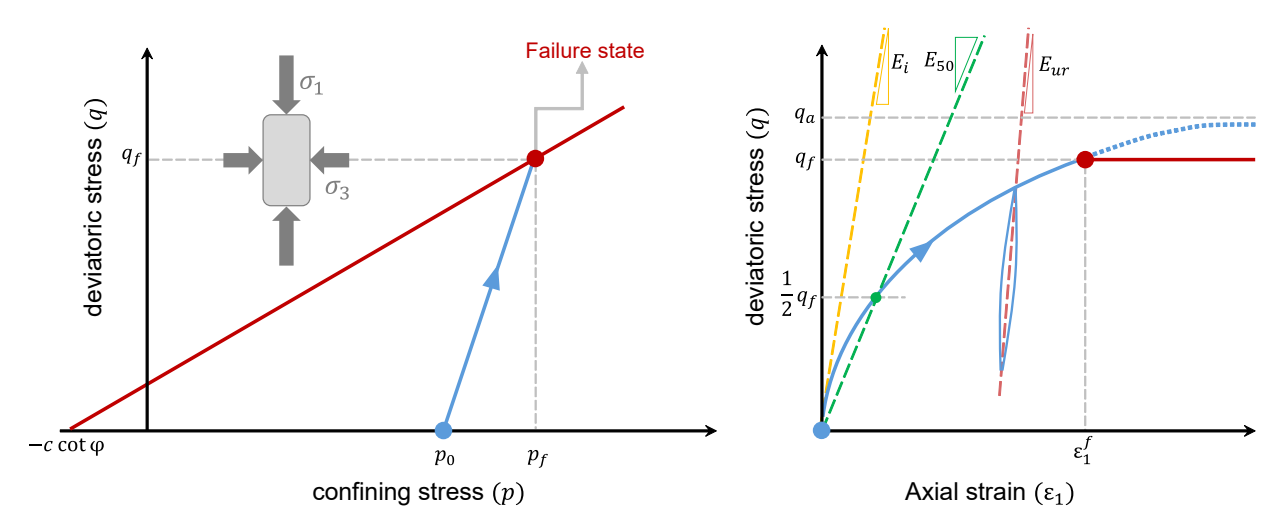


Figure 2. Stress-strain response under triaxial conditions.

Note the following in reference to Figure 3:

- 1. The cap yield surface is revealed as an ellipse in q:p' stress space with an aspect ratio of M
- An oedometer (1D compression) stress path intersects and expands the size of the cap yield surface when the soil yields; that is, transitions from elastic to elastic-plastic behaviour.
- 3. The stress-strain behavior of the sample in an oedometer test is defined by a tangent stiffness called the oedometer stiffness  $^{E}_{oed}$ . Like other stiffness quantities,  $^{E}_{oed}$  is not constant but its value depends on the stress of the sample.

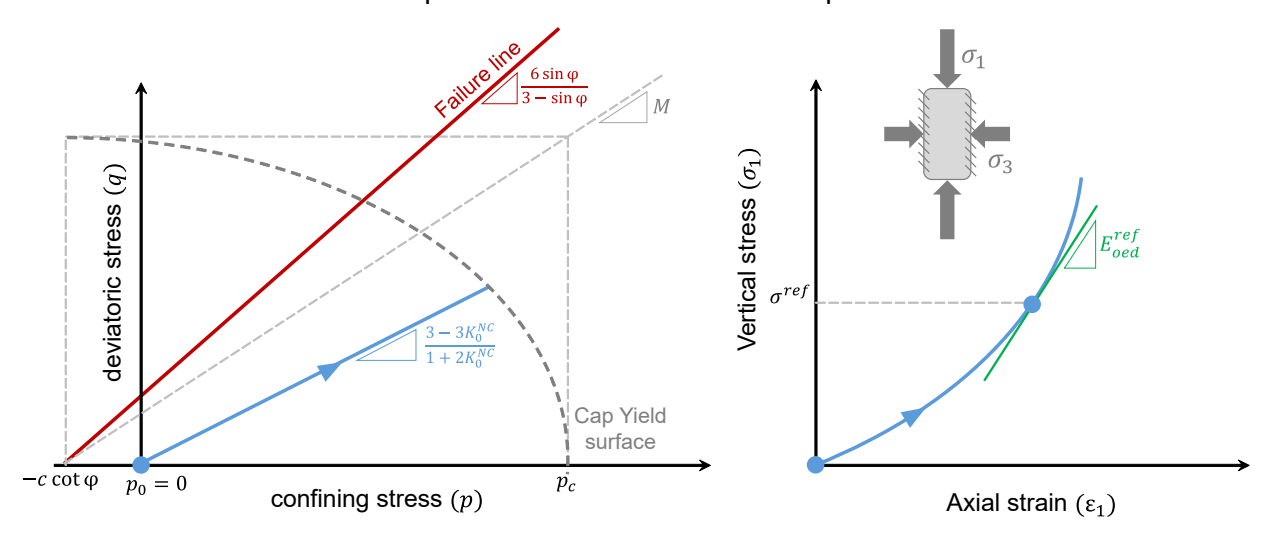


Figure 3. Stress-strain response under 1D compression oedometer loading.

Note the following in reference to Figure 4 and Figure 5 (note: the model's constants are highlighted in light grey):

- 1. The  $q:\mathcal{E}_1$  stress-strain path is approximated by a hyperbolic curve until the stress path intersects the Mohr-Coulomb failure surface (Figure 4).
- 2. Failure occurs before the curve reaches its asymptotic value. The difference between failure and asymptotic stresses is determined by constant  $^{R}f$ .



- 3. The stress-strain behaviour at the beginning of loading is controlled by the initial tangent stiffness  $^{E}i$ . This stiffness value is, however, difficult to measure, so it is calculated from another, more easily measured half-failure secant stiffness  $^{E}50$ .
- 4. The half-failure secant stiffness is a stress-dependent stiffness that depends on the minimum principal stress  $\sigma_3$ .
- 5. A similar stress-dependency is also considered in the Hardening Soil model for the unloading-reloading stiffness  $E_{ur}$ .
- 6. The slope of the oedometer stress path is a function of the coefficient of lateral pressure  $K_0^{nc}$  (Figure 5).
- 7. The cap yield surface in q:p' space is an ellipse with a horizontal major axis. In a non-cohesive soil, this elliptical yield surface is centered around  $p = -c\cot \varphi$ ; however, SIGMA/W's implementation centres the ellipse on the origin regardless of the cohesion value.
- 8. The oedometer stiffness is also a stress-dependent stiffness presented in terms of the vertical stress  $\sigma_1$ .

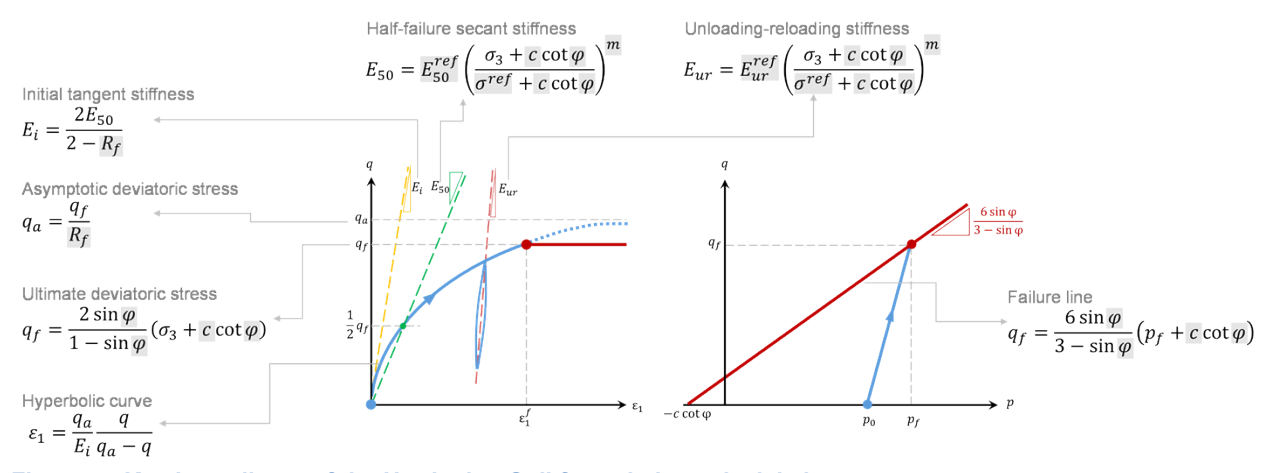


Figure 4. Key ingredients of the Hardening Soil formulation: triaxial shear.

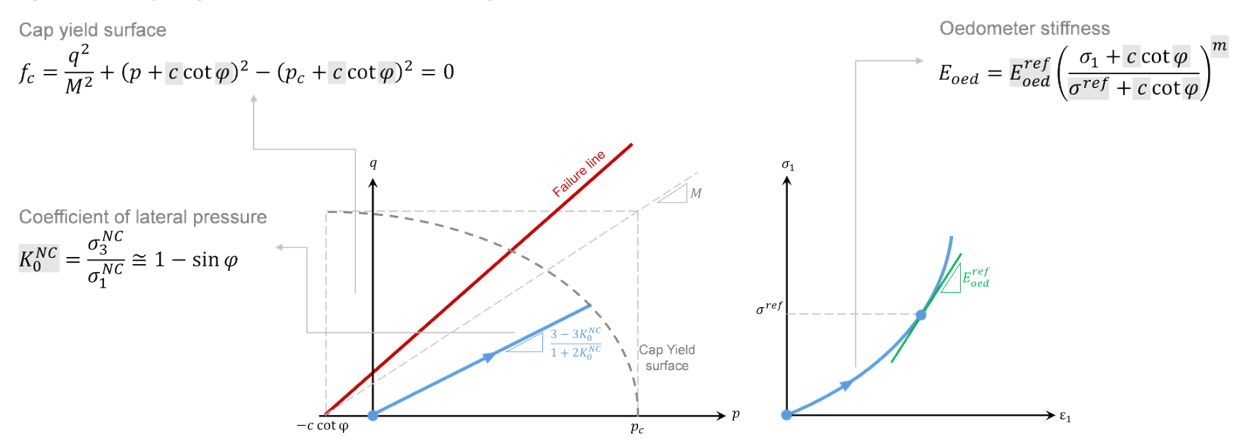


Figure 5. Key ingredients of the Hardening Soil formulation: one-dimensional compression. .

Table 1 summarizes the parameters of the Hardening Soil model:



**Table 1. Parameters for the Hardening Soil model** 

Parameter	Symbol	Unit
Effective angle of shear resistance	$\phi^{'}$	o
Effective cohesion	c <sup>'</sup>	kPa
Angle of dilation	ψ	o
Reference unload-reload stiffness (via drained triaxial)	$E'^{ref}_{ur}$	kPa
Reference secant stiffness (via drained triaxial); $q=0.5(q_f)$	$E^{'ref}_{50}$	kPa
Reference tangent stiffness in primary oedometer loading	E'ref oed	kPa
Unload-reload Poisson's ratio	$v'_{ur}$	
Exponent controlling stiffness stress dependency	m	
Reference confining stress for stress dependent stiffness calculations	$p^{ref}$	kPa
Failure ratio $q_f/q_a$	$R_f$	
Over consolidation ratio	OCR	
Coefficient of earth pressure for the normally compressed state	$K_0^{nc}$	
Initial void ratio	е	

# **Parameterization Procedure**

Figure 6 provides a conceptual workflow for the procedure. The parameterization procedure is premised on availability of drained triaxial test results and, ideally, oedometer compression tests. The parameterization procedure produces the constants for a specific constitutive model. These constants are then used as inputs for the model used in a numerical simulation. Finally, the parameterization is verified by comparing the simulated and measured results.



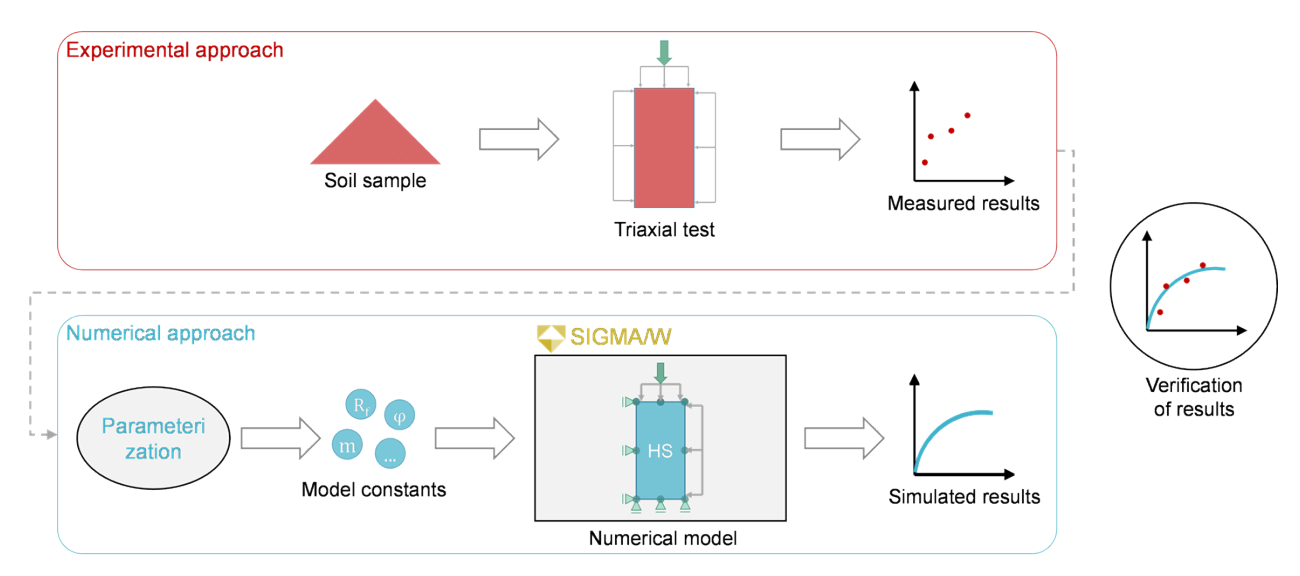


Figure 6. Conceptual workflow of the parameterization procedure.

#### Step 1

The first step is to determine the effective friction angle  $\varphi$  and the effective cohesion c (Figure 7). The failure states from numerous triaxial tests at different confining pressures are located on the Mohr-coulomb failure line in p-q space. As such, the slope  $(\tan\beta)$  as well as the y-intercept  $(\alpha)$  of the failure line is calculated using the method of least squares, where n is the number of data points. The effective friction angle and the effective cohesion of the soil can be found by changing the coordinate system to a shear-normal stress space.

$$\tan\beta = \frac{n\sum p_f q_f - \sum p_f \sum q_f}{n\sum p_f^2 - \left[\sum p_f\right]^2}$$
 Equation 1 
$$\alpha = \frac{\sum p_f^2 \sum q_f - \sum p_f q_f \sum p_f}{n\sum p_f^2 - \left[\sum p_f\right]^2}$$
 Equation 2 
$$\varphi = \sin^{-1}\frac{3\tan\beta}{6 + \tan\beta}$$
 Equation 3 
$$c = \frac{\alpha\tan\varphi}{\tan\beta}$$



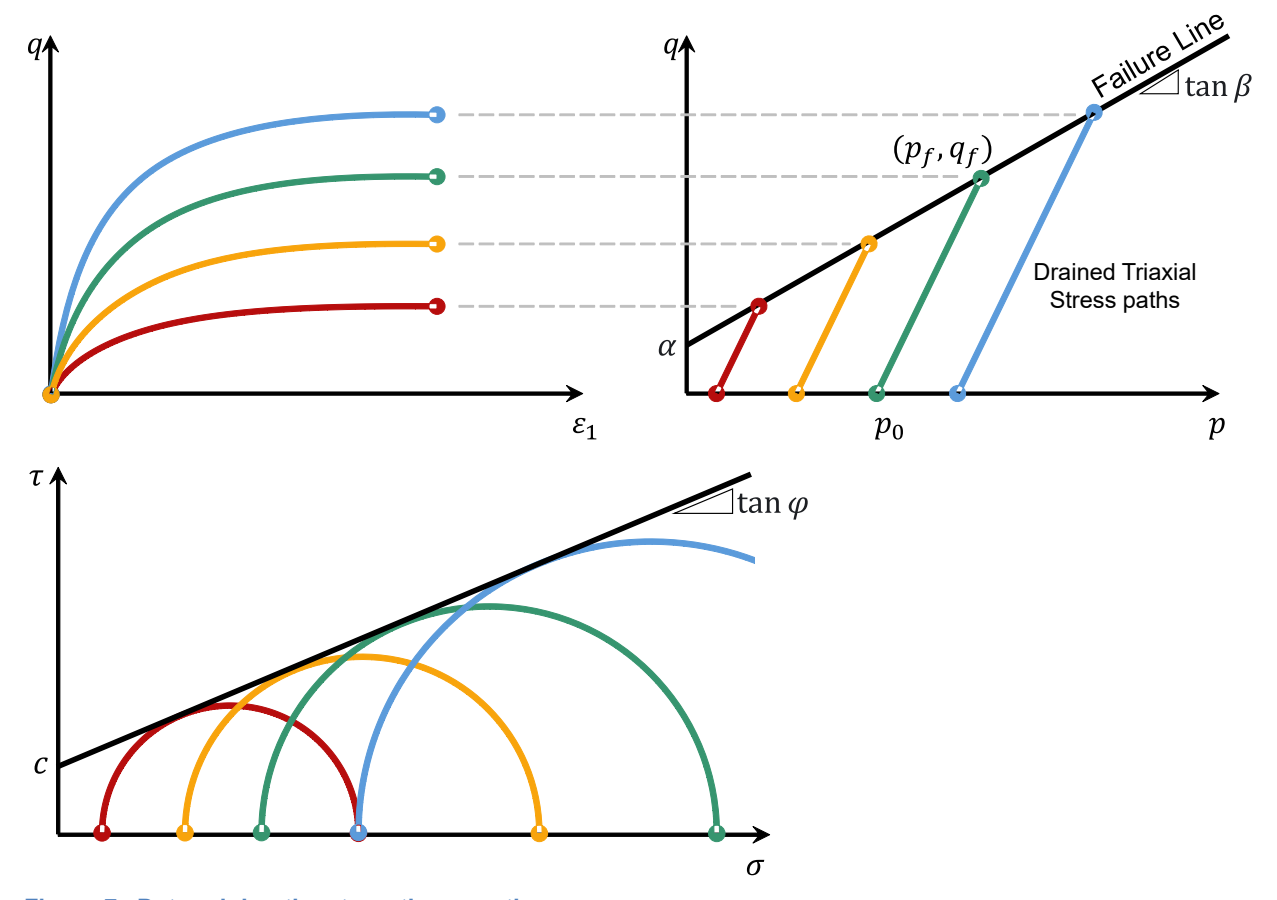


Figure 7. Determining the strength properties.

#### Step 2

The second step is to consider a reference stress, and to estimate reference stiffness parameters (Figure 8). The results of a particular triaxial test are used to obtain the reference parameters. The confining pressure of this test the reference stress. The failure deviatoric stress for this particular test is determined based on Mohr-Coulomb Strength constants determine in step 1. The half-failure reference stiffness is the slope of a straight line that passes through the point carrying 50 percent of the failure deviatoric stress. The least squares method is applied again on the unloading-reloading branch of the stress-strain curve to calculate the unloading-reloading reference stiffness.

$$q^{ref}_{f} = \frac{2\sin\varphi}{1-\sin\varphi}(\sigma^{ref}+c\cot\varphi)$$
 Equation 5 
$$E^{ref}_{50} = \frac{\frac{1}{2}q^{ref}_{f}}{\varepsilon_{1}^{50}}$$
 Equation 6 
$$E^{ref}_{ur} = \frac{n\sum\varepsilon_{1}q_{ur}-\sum\varepsilon_{1}\sum q_{ur}}{n\sum(\varepsilon_{1})^{2}-\left[\sum\varepsilon_{1}\right]^{2}}$$



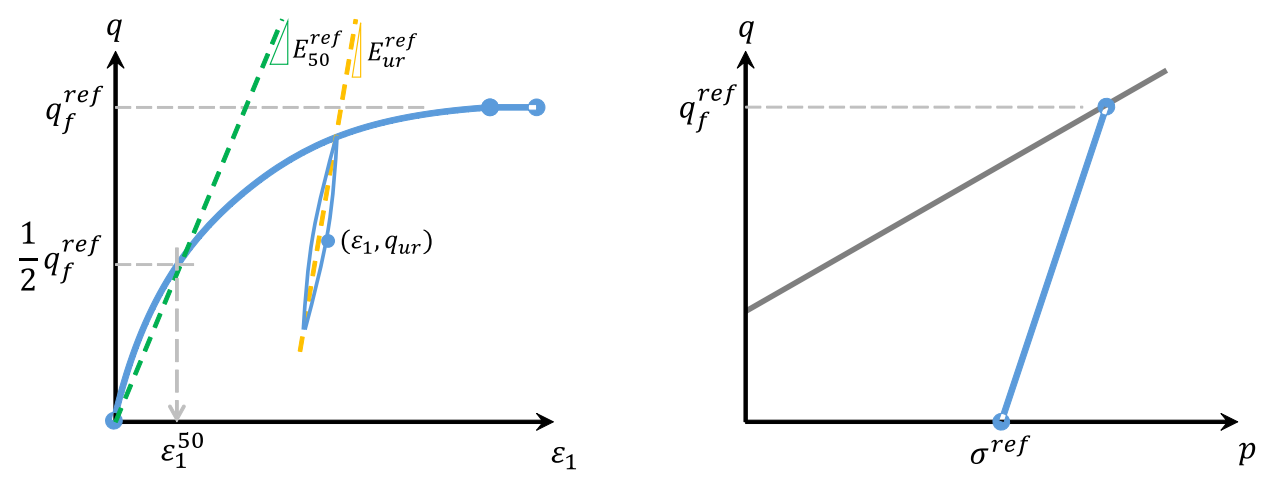


Figure 8. Determining the reference stress and stiffness parameters  $E^{ref}_{\ 50}$  and  $E^{ref}_{\ wr}$  .

#### Step 3

The third step is to determine the stress dependency exponent m (Figure 9). In stress-strain curves of drained triaxial tests with different confining pressures, half-failure stiffness parameters are first calculated using the method described in step 2. A new natural logarithmic space can then be defined that represents the half-failure stiffness of each test in the form of a single point. The point corresponding to the reference test is located on the origin in this new space. The stress dependency exponent, m is the slope of a trend line that passes through these points. The same steps can be followed for unloading-reloading phases in order to calculate the stress dependency exponent of the unloading-reloading stiffness. In the Hardening soil model, however, it is assumed that the constant m is the same for stiffness parameters.

$$E_{50} = E_{50}^{ref} \left( \frac{\sigma_3 + c\cot \varphi}{\sigma^{ref} + c\cot \varphi} \right)^m$$

$$\left[ \ln \frac{E_{50}}{E_{50}^{ref}} \right] = m \left[ \ln \frac{\sigma_3 + c\cot \varphi}{\sigma^{ref} + c\cot \varphi} \right]$$

$$Equation 9$$

$$m = \frac{\sum x_i y_i}{\sum x_i^2}$$
Equation 10



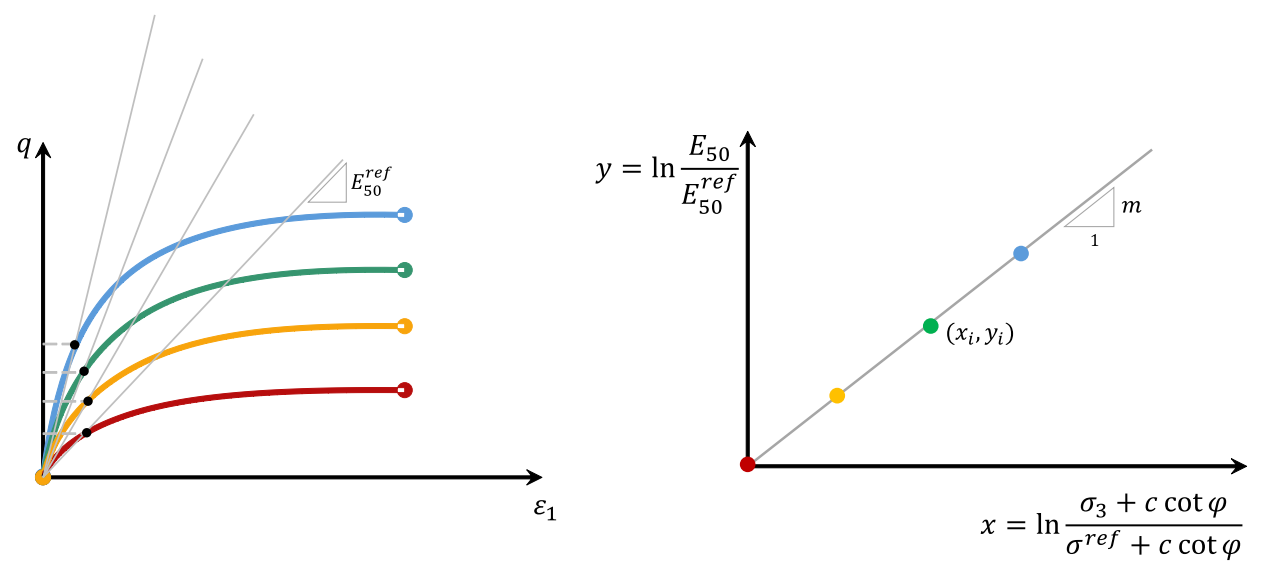


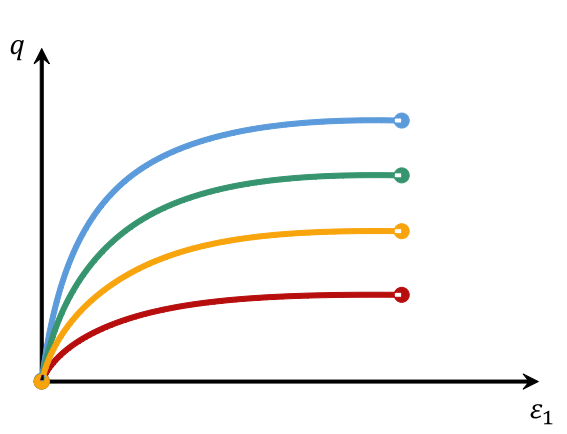
Figure 9. Determining the stress dependency exponent m.

#### Step 4

The fourth step is to determine the failure ratio  $^Rf$  (Figure 10). This constant has a value between 0.5 and 1 and is usually assumed to be 0.9. A more accurate value for this constant, however, can be calculated based on the results of triaxial tests. First, the stress-strain hyperbolic function is rewritten in terms of the failure ratio  $^Rf$ . This expression introduces a new coordinate system in which each hyperbolic curve is projected to a straight line. The failure ratio  $^Rf$  is the slope of these parallel lines.

$$R_f = \frac{q_f}{q_a}$$
 Equation 11 
$$\varepsilon_1 = \frac{q_f}{\frac{1}{E_i q_f} - R_f}$$
 Equation 12 
$$y = R_f x + b \rightarrow \varepsilon_1 \frac{q_f}{q} = R_f \varepsilon_1 + \frac{q_f}{E_i}$$
 Equation 13





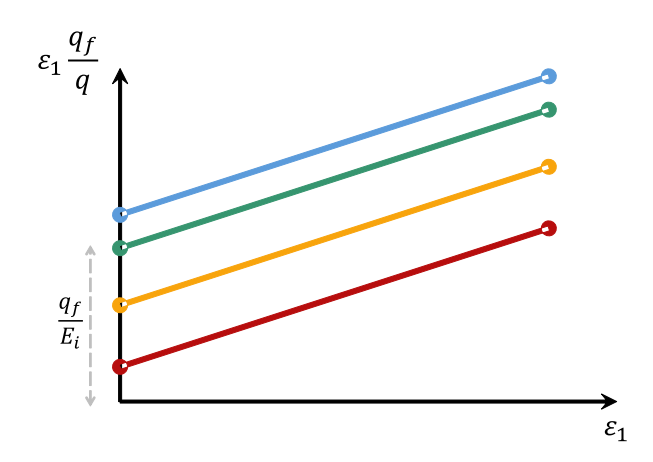


Figure 10. Determining the failure ratio  $^{R}/.$  Step 5

The fifth step is to determine the reference oedometer stiffness  $E_{oed}^{ref}$  (Figure 11). The coefficient of lateral pressure can also be estimated from the same data. The oedometer test result is required for this step; however, these values can be approximated in the case where the appropriate laboratory result is not available. As mentioned earlier, the oedometer reference stiffness is defined in a one-dimensional compression test. By definition, it is the tangent stiffness at the point where the vertical stress is equal to the reference stress. In addition, the coefficient of lateral pressure for a normally consolidated soil  $E_{oed}^{NC}$  is the ratio of lateral stress  $E_{oed}^{NC}$  to the vertical stress  $E_{oed}^{NC}$  in an oedometer test. An estimate of  $E_{oed}^{NC}$  and  $E_{oed}^{NC}$  is given by Equation 14 and Equation 15, respectively.

$$0.5~E_{50}^{ref} < E_{oed}^{ref} < 0.8E_{50}^{ref}$$
 Equation 14 
$$K_0^{NC} \cong 1 - \sin \varphi$$
 Equation 15

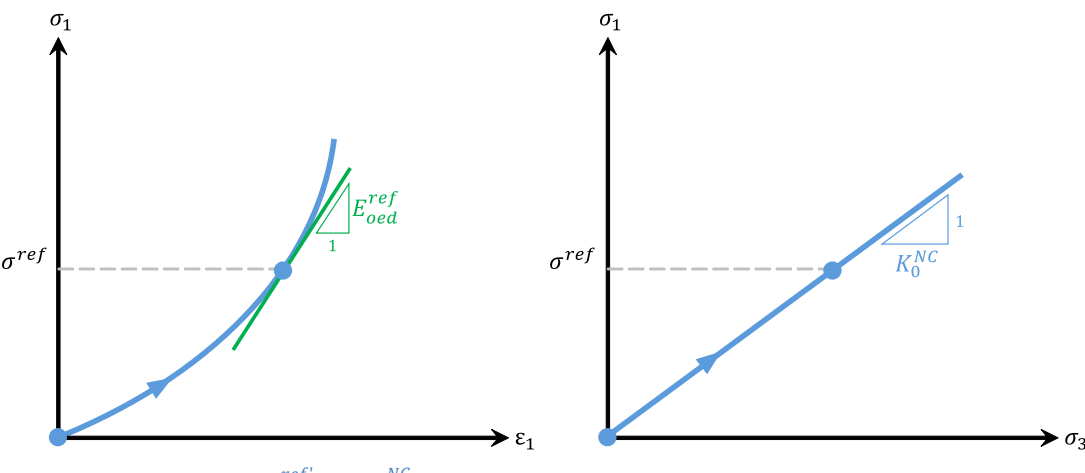


Figure 11. Determining  $E_{oed}^{ref'}$  and  $K_{0}^{NC}$ .



# **Application**

Figure 12 shows the results from numerous triaxial tests conducted on Ottawa Sand at various confining pressures (Krachtoudi, 2001). Figure 13 to Figure 17 summarize the parameterization procedure as applied to the results of these tests. Table 2 provides a summary of the model constants obtained from the parameterization procedure. Note that neither the OCR nor Poisson's ratio could be parameterized because all specimens were normally compressed and the data required to determine Poisson's ratio was not available.

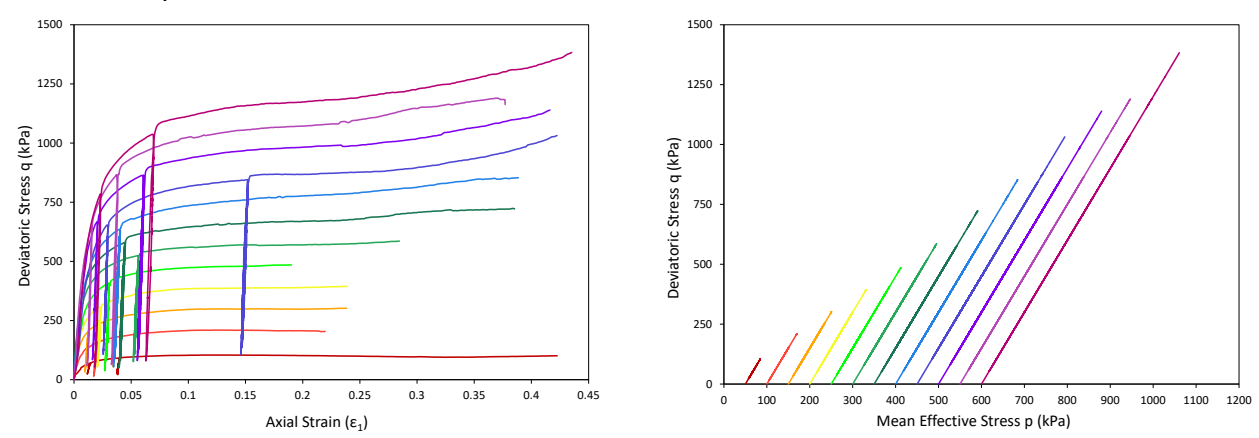


Figure 12. Triaxial test results on Ottawa Sand (Krachtoudi, 2001).

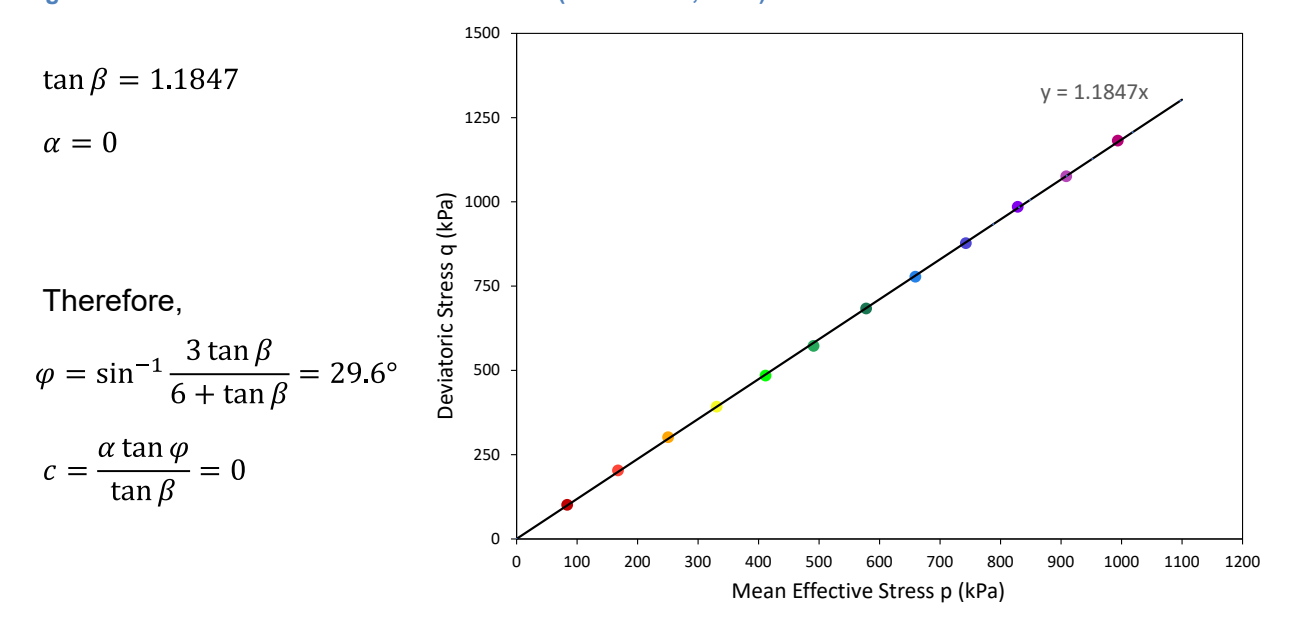


Figure 13. Step 1: determination of the strength properties.

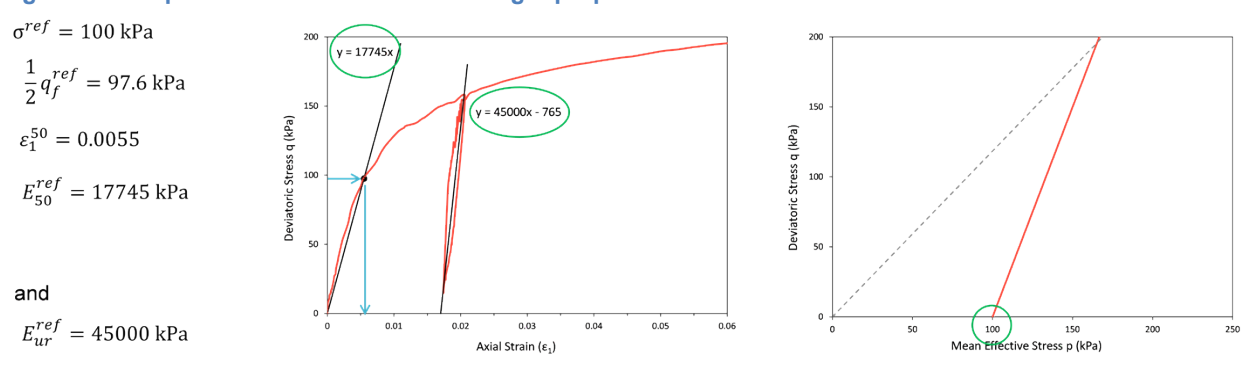


Figure 14. Step 2: determination of the reference stress and stiffness parameters  $E_{50}^{ref}$  and  $E_{ur}^{ref}$ 

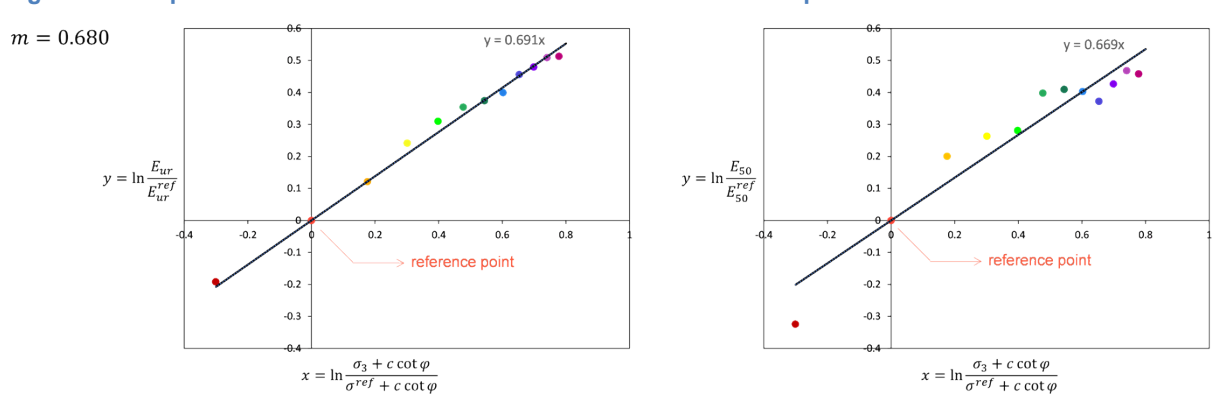


Figure 15. Step 3: determination of the stress dependency exponent m.

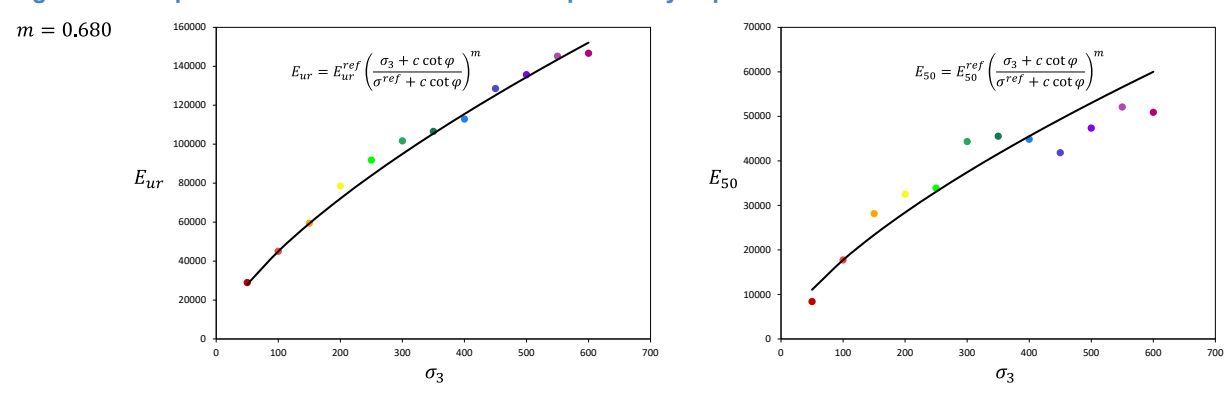


Figure 16. Step 3: verification of the stress dependency exponent m.

The near vertical branches of the curves in Figure 17 represent unloading-reloading phases and are not included in the linear regression to obtain  $^{R}f$ .

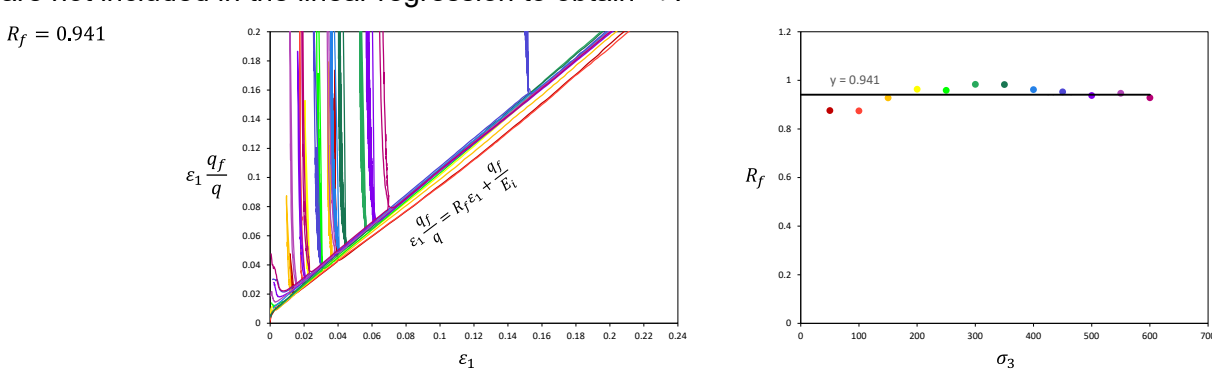


Figure 17. Step 4: determination of the failure ratio  $^R$ f.



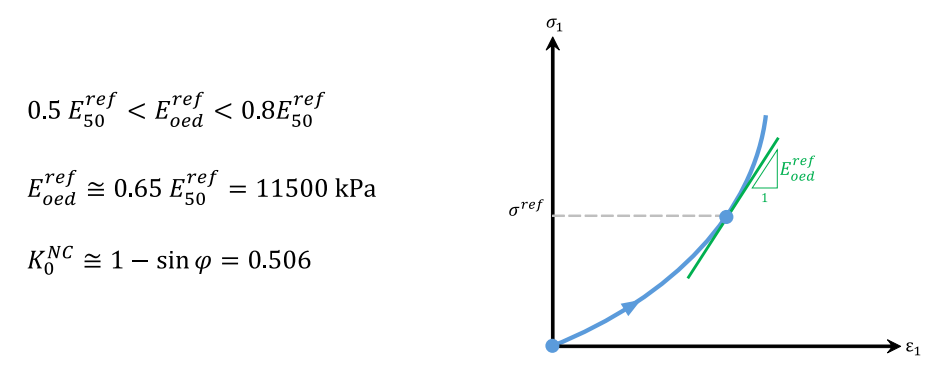


Figure 18. Step 5: Estimation of  $E^{ref^{\,\prime}}_{oed}$  and  $K^{NC}_{\phantom{MC}0}$ 

Table 2. Ottawa sand model constants for the Hardening Soil model

Parameter	Symbol		Unit
Effective angle of shear resistance	$\phi^{'}$	29.6	o
Effective cohesion	c <sup>'</sup>	0	kPa
Angle of dilation	ψ	N/A	o
Reference unload-reload stiffness (via drained triaxial)	E' <sup>ref</sup> ur	45000	kPa
Reference secant stiffness (via drained triaxial); $q=0.5(q_f)$	E' <sup>ref</sup> 50	17745	kPa
Reference tangent stiffness in primary oedometer loading	E'ref oed	11500	kPa
Unload-reload Poisson's ratio	ν' <sub>ur</sub>	0.2	
Exponent controlling stiffness stress dependency	m	0.68	
Reference confining stress for stress dependent stiffness calculations	$p^{ref}$	100	kPa
Failure ratio $q_f/q_a$	$R_f$	0.941	
Over consolidation ratio	OCR	1.0	
Coefficient of earth pressure for the normally compressed state	$K_{0}^{nc}$	0.506	
Initial void ratio	е	N/A	

# **Verification**

Figure 19 and Figure 20 compare the simulated, analytical, and measured results for the 12 triaxial tests on Ottawa Sand (Krachtoudi, 2001). Colored curves are laboratory results and continuous black lines are the results of the SIGMA/W simulations. The analytical results of the



Hardening Soil model are also shown in these diagrams as orange dashed lines. Refer to the associated GeoStudio project file to explore the analysis definitions and simulated results in detail.

The full compatibility of analytical and simulated curves shows the reliability of the model's implementation in SIGMA/W. In addition, the acceptable consistency between the laboratory results and simulations indicates the capabilities of the calibrated Hardening Soil model in predicting the responses of the sand samples. The parameterization procedure relies on linear regression; consequently, the simulated/analytical results will generally provide a better fit to those specimens with measured data that was nearest the trend lines.

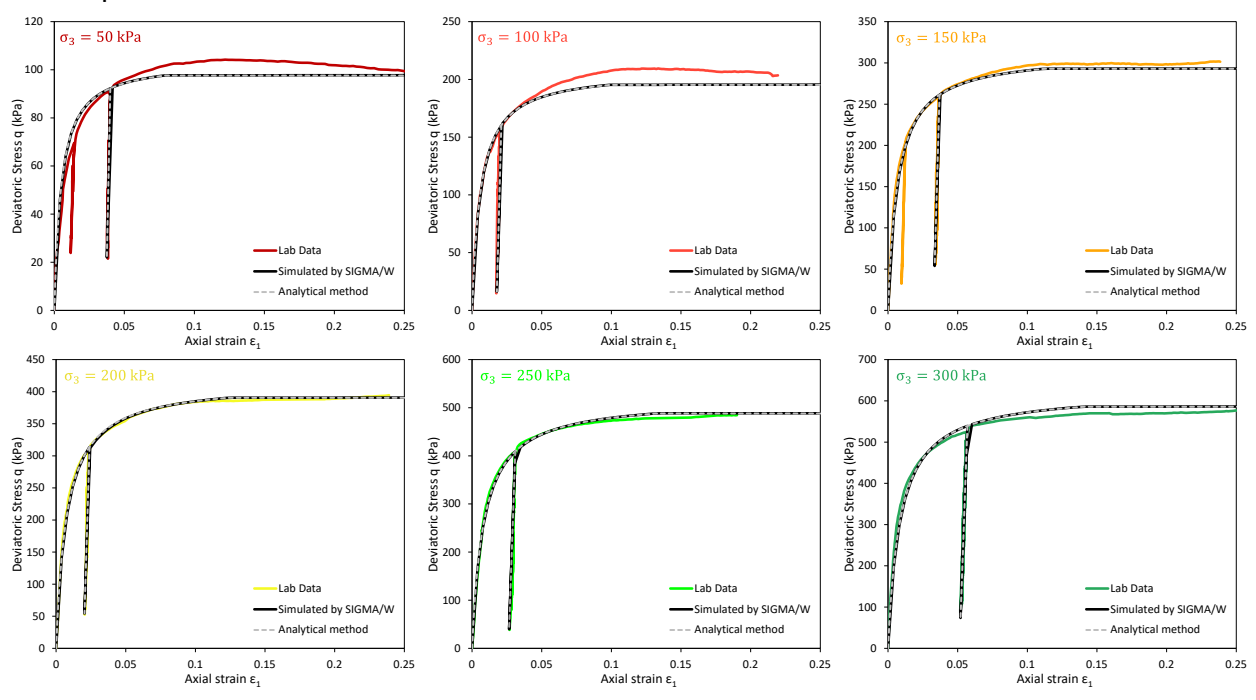


Figure 19. Comparison of simulated, analytical, and measured results for specimen with confining pressures less than 350 kPa.



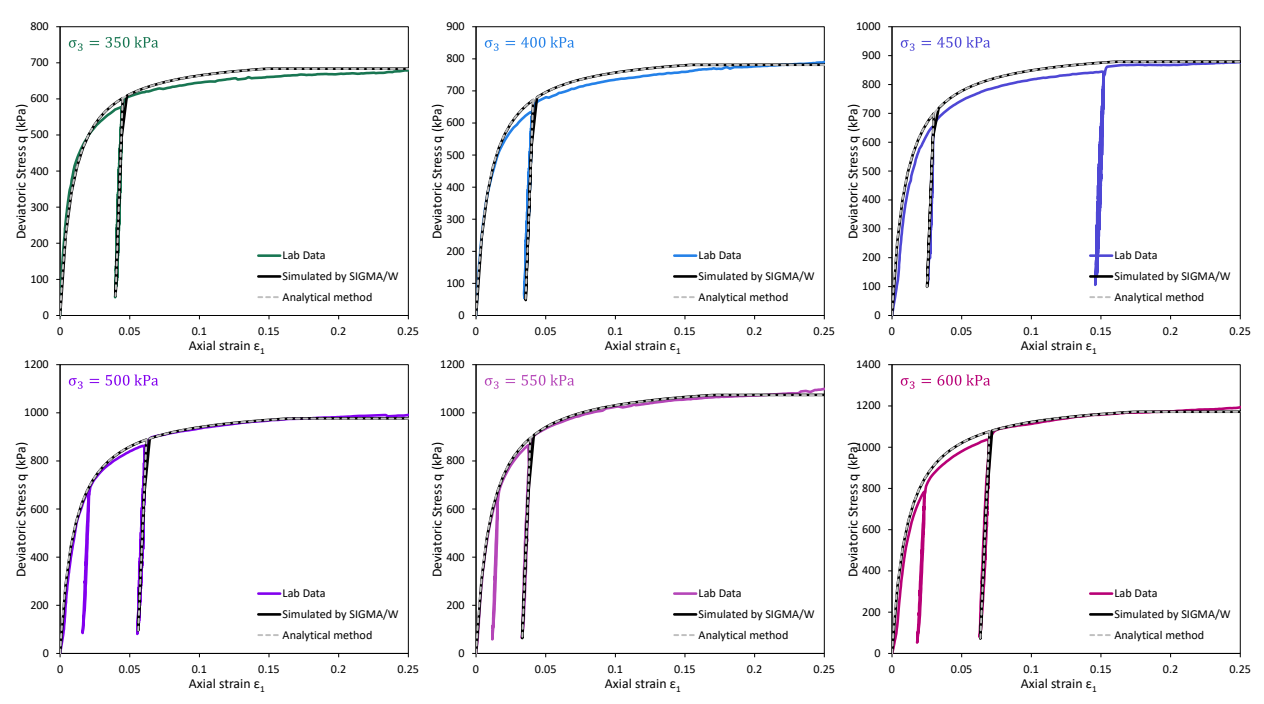


Figure 20. Comparison of simulated, analytical, and measured results for specimens with confining pressure of 350 kPa and greater.

# **Summary**

The calibration procedure of the Hardening Soil material model was provided in five straight forward steps. The results of the drained triaxial tests have shown to be the only laboratory dataset required for parameterizing the model; however, oedometer tests are ideally also

available to parameterize  $E_{\it oed}^{\it ref}$ . The material constants were used in numerical simulations and the results were found to compare favorably with both the analytical solution and corresponding laboratory results.

# References

Krachtoudi, C.Z., 2011. Numerical simulation of the response of Ottawa sand in the triaxial and the torsional shear apparatus (Master's thesis). National Technical University of Athens.

Schanz, T., Vermeer, P.A. and Bonnier, P.G., 1999. The hardening soil model: formulation and verification. Beyond 2000 in computational geotechnics, pp.281-296.

Seequent ULC. 2024. Stress-strain modeling with GeoStudio. Calgary, Alberta, Canada.

